Inhibition of human copper trafficking by a small molecule significantly attenuates cancer cell proliferation

Jing Wang[1,6,†], **Cheng Luo**[2,†], **Changliang Shan**[3,†], **Qiancheng You**[1,6,†], **Junyan Lu**[2], **Shannon Elf**[3], **Yu Zhou**[2], **Yi Wen**[2], **Jan L. Vinkenborg**[4], **Jun Fan**[3], **Heebum Kang**[3], **Ruiting Lin**[3], **Dali Han**[1,6], **Yuxin Xie**[1,6], **Jason Karpus**[1,6], **Shijie Chen**[2], **Shisheng Ouyang**[2], **Chihao Luan**[5], **Naixia Zhang**[2], **Hong Ding**[2], **Maarten Merkx**[4], **Hong Liu**[2], **Jing Chen**[3,*], **Hualiang Jiang**[2,*], and **Chuan He**[1,6,*]

[1]Department of Chemistry, Department of Biochemistry and Molecule Biology, Institute for Biophysical Dynamics, The University of Chicago, 929 East 57th Street, Chicago, Illinois 60637, USA [2]Drug Discovery and Design Center, State Key Laboratory of Drug Research, Shanghai Institute of Materia Medica, Chinese Academy of Sciences, Shanghai 201203, China [3]Department of Hematology and Medical Oncology, Winship Cancer Institute of Emory, Emory University School of Medicine, Atlanta, Georgia 30322, USA [4]Laboratory of Chemical Biology, Eindhoven University of Technology, 5600 MB Eindhoven, Netherlands [5]Department of Molecular BioSciences, Northwestern University, Evanston, Illinois 60208, USA [6]Howard Hughes Medical Institute, The University of Chicago, 929 East 57th Street, Chicago, Illinois 60637, USA

Abstract

Copper is a transition metal that plays critical roles in many life processes. Controlling the cellular concentration and trafficking of copper offers a route to disrupt these processes. Here we report small molecules that inhibit the human copper-trafficking proteins Atox1 and CCS, and so provide a selective approach to disrupt cellular copper transport. The knockdown of Atox1 and CCS or their inhibition leads to a significantly reduced proliferation of cancer cells, but not of normal cells, as well as to attenuated tumour growth in mouse models. We show that blocking copper trafficking induces cellular oxidative stress and reduces levels of cellular ATP. The reduced level of ATP results in activation of the AMP-activated protein kinase that leads to reduced lipogenesis. Both effects contribute to the inhibition of cancer cell proliferation. Our results establish copper chaperones as new targets for future developments in anticancer therapies.

Copper is a redox-active transition metal essential for most living organisms and serves as a catalytic cofactor for enzymes that function in antioxidant defence, iron homeostasis, cellular respiration and a variety of biochemical processes. However, intracellular free copper must be strictly limited because of its potential toxic side effects. The uncontrolled accumulation of copper could lead to increased oxidative stress and inappropriate binding to macromolecules. Most cells evolve complex systems of copper regulation and trafficking to satisfy the cellular copper requirements and simultaneously minimize the potential toxicity[1,2].

Once copper enters the cytoplasm, it is bound by cytosolic copper chaperones such as CCS and Atox1, which then transfer copper to specific cellular destinations. Copper transfer is mediated through protein–protein interaction and ligand exchange between the chaperone and the target protein[3,4]. Atox1 binds Cu(I) with a conserved CXXC motif and delivers copper to the N-terminal metal-binding domains of ATP7A and ATP7B in the secretory pathway[5], which includes the *trans*-Golgi network[6]. CCS transfers copper to the antioxidant enzyme Cu/Zn superoxide dismutase (SOD1) using a CXXC-containing copper-binding domain[7–10] that is structurally homologous to Atox1[11–14]. Low oxygen concentrations also promote CCS mitochondrial localization to protect cells on the superoxide released from the incomplete reduction of oxygen in mitochondria[2,15,16].

Also, an increasing amount of evidence suggests that copper plays a significant role in the control of normal endothelial cell growth in wound healing[17] and cancer. Copper has long been recognized as an important factor in mammals for its ability to mount an angiogenic response[18–20]; incubation with copper also induces an improved mobility in endothelial cells. In numerous cancerous tissues and serums, the concentration of copper is shown to exceed that of normal tissues[21], but the detailed molecular mechanisms are not completely understood. A recent study indicated that Atox1 knockdown inhibits copper-stimulated proliferation of lung carcinoma cells[22]. Here we present organic molecules that target copper-trafficking proteins Atox1 and CCS and show that the copper-delivery functions of these copper chaperones are critical to cancer cell proliferation. The knockdown of these proteins or their selective inhibition effectively reduces the proliferation of cancer cells and significantly attenuates tumour growth in xenograft mice models. We further investigated the underlying mechanisms that indicate the critical roles of copper trafficking in cancer cells.

Results

Inhibition of Atox1 and CCS with small molecules

To investigate the impacts of copper trafficking on cancer cell proliferation and to elucidate the underlying mechanisms, we set out to develop organic small molecules that inhibit the human copper chaperones Atox1 and CCS. We envisioned that these molecules could be used to block cellular copper trafficking to reveal the potential responses of cancer cells (Fig. 1a).

As Atox1 and domain I of CCS share a similar βαββαβ-protein fold structure[11–13] and copper-binding site[23,24] (Fig. 1b and Supplementary Fig. 3a), we aimed to find small molecules that may block the potential copper-transfer interfaces essential to the activity of copper-dependent enzymes. We performed a hierarchical virtual screening strategy based on characterized structures and the established copper-transfer mechanism (Fig. 1c). DOCK4.0[25] was used for the screening of the Specs database, which contains more than 200,000 compounds. Out of this screen, and based on the structural features, physical chemistry properties and drug-like characteristics, 237 compounds were selected for more bioactivity testing (see Methods for more details).

To validate small molecules identified in the virtual screening, we utilized a previously developed fluorescence resonance energy transfer (FRET)-based probe named eCALWY3[26] to examine the inhibition effects of these 237 candidates. The eCALWY3 probe used in this study consists of Atox1 and domain 4 of its copper-binding partner ATP7B (WD4) fused to the FRET partner fluorescent proteins (excitation at 433 nm and emissions at 475 nm and 527 nm) and connected through a long flexible linker; Atox1 delivers Cu(I) to WD4 through protein–protein recognition and Cu(I) exchange via conserved Cys residues in both proteins. Binding of either Cu(I) or Zn(II) is known to induce a twofold decrease of the FRET ratio in eCALWY3, although Cu(I) is the biologically relevant metal of this complex. We envisioned that a small molecule that specifically binds at the interface would inhibit the metal-mediated formation of the complex between Atox1 and WD4, which would lead to an increased FRET ratio similar to that of the apo form of eCALWY3.

Six compounds (at 100 μM) exhibited inhibition of the Atox1– WD4 interaction in the presence of metal (Fig. 1d, Supplementary Fig. 1 and Supplementary Table 1). Treatment with these small molecules markedly reduced cell proliferation in several human cancer cell lines tested, including lung cancer H1299, head and neck cancer 212LN, and breast cancer MB231 cells (Supplementary Fig. 2a–c). Minimal effects were observed in several normal cells, such as normal human PIG1 melanocyte cells and normal human dermal fibroblasts (HDF) cells (Supplementary Fig. 2d,e). Taking into account both the FRET screening and cell-killing assay, **DC_AC2** and **DC_AC50** were selected as the two best candidates for our studies. **DC_AC2** was later shown to be toxic in mice experiments, which led us to focus on **DC_AC50**.

Binding of DC_AC50 to Atox1 and CCS

To look for the direct binding of **DC_AC50** to its target proteins, we expressed and purified Atox1, full-length CCS and domain I of *CCS* in *E. coli*. We discovered that **DC_AC50** is a self-fluorescing compound with excitations at 290 nm and 355 nm, and emission at 494 nm (Supplementary Fig. 3b); the excitation and emission wavelengths are different from those of eCALWY3 used in the previous FRET measurement. As a result of the intrinsic fluorescence of **DC_AC50**, we anticipated that a FRET between Atox1/CCS and **DC_AC50** could occur. As shown in Fig. 2a,b, Atox1 and full-length CCS display their maximum fluorescent signals at 335 and 350 nm, respectively, when excited at 278 nm in the absence of **DC_AC50**. With the addition of **DC_AC50**, the peak at 335 or 350 nm, which corresponds to the emission of Tyr or Trp, respectively, was reduced, whereas the emission

of **DC_AC50** at 494 nm was elevated. As the emission intensity at 335 or 350 nm depends on the molar ratio of protein–**DC_AC50** versus protein, the binding affinities of the protein to the small molecule could be calculated through this measurement (K_d, ∼6.8 μM for Atox1 and ∼8.2 μM for full-length CCS) (Fig. 2c,d). Also, we applied fluorescence anisotropy (FA) to measure the binding affinities of **DC_AC50** to Atox1 and CCS. To 1 μM of **DC_AC50** we added increasing concentrations of Atox1, full-length CCS and domain I of CCS with excitation at 355 nm. Fluorescent emission at 494 nm was recorded and the FA changes were used to obtain accurate K_d values of 6.4 μM for Atox1, 7.9 μM for full-length CCS and 12.2 μM for CCS domain I (Supplementary Fig. 3c,d). These K_d values corroborated the affinities measured by FRET. Finally, surface plasmon resonance (SPR) was used to confirm the binding of the small molecule to these proteins (Supplementary Fig. 3e,f).

Computational models were built to reveal the potential binding modes of **DC_AC50** to Atox1 and to domain I of CCS, and these indicated that **DC_AC50** was bound with similar conformations to both targets (Fig. 2e,f). The binding sites of the small molecule are located at the potential copper-transfer interfaces of these chaperone proteins but not on the copper-binding cysteine residues (Cys12 and Cys15 for Atox1, and Cys22 and Cys25 for CCS); binding of the small molecule would disrupt the copper-transfer function of these two chaperones by inhibiting protein–protein interactions. According to the model, the side chains of residues Glu17, Arg21 and Lys60 in Atox1 form three hydrogen bonds with the heteroatoms of **DC_AC50**, whereas the side chains of Val22, Ala35 and Thr58 form hydrophobic packing with the substituted phenyl group of **DC_AC50** (Fig. 2e). As for the interaction between domain I of CCS and **DC_AC50**, the side chains of Asp27 and Lys31, which in Atox1 correspond to Glu17 and Arg21, respectively, also form two hydrogen bonds with the small molecule (Fig. 2f). Ser24, which occurs as a glycine (Gly14) in the corresponding site of Atox1, forms an additional hydrogen bond with the amino group of **DC_AC50**. In addition, the side chains of Ala28, Ser32 and Thr69 may take part in hydrophobic packing between domain I of CCS and **DC_AC50** (Fig. 2f).

To characterize the binding further, we performed a [1]H-^{15}N heteronuclear single-quantum correlation NMR titration of **DC_AC2** to Cu(I)-free Atox1. **DC_AC2** has the same core structure as **DC_AC50** and has a higher solubility in water than **DC_AC50**, which results in better NMR signals for this study. The NMR data clearly revealed the interactions between Cu(I)-free Atox1 and **DC_AC2** (Supplementary Fig. 4a). The addition of **DC_AC2** into the solution of Cu(I)-free Atox1 significantly perturbed and attenuated the following residues with chemical shifts: Ser7, Ala18, Val19, Ser20, Val22, Leu23, Lys25, Gly27, Val29, Lys30, Asn37, Lys38, Glu43, His46, Met48, Thr50, Leu52, Ala53, Leu55, Lys57, Thr58 and Gly59. The perturbed residues localized to α-helices 1 and 2 (Supplementary Fig. 4b), which indicates that the interface that constituted two helices modulates the binding of **DC_AC2** to Cu(I)-free Atox1.

In addition, **DC_AC2** exhibited similar binding behaviour to both Cu(I)-loaded Atox1 and apo-Atox1 (Supplementary Fig. 4c, d), which suggests that the Cu(I) ion is not required for the interaction between Atox1 and DC_AC2. In fact, the addition of Cu(I) caused the expected chemical shift changes of residues in the copper-binding motif of [11]TCGGCA[16] of

Atox1 regardless of the presence of **DC_AC2** (Supplementary Fig. 4e). Based on the aforementioned NMR titration data, a structure model for the complex of Atox1 bound with either **DC_AC2** or **DC_AC50** was generated (Supplementary Fig. 4f).

To support the computational models, we constructed several Atox1 and full-length CCS mutants by replacing selected residues with Ala (Glu17A, Arg21A, Val22S, Lys60A and Thr58A in Atox1, and Ser24A, Asp27A, Lys31A, Ser32A and Thr69A in full-length CCS). As shown in Supplementary Fig. 5a,b, the mutation of these amino acids weakened the binding affinities (three- to sixfold) of **DC_AC50** to the mutant protein as compared with the wild-type Atox1 and CCS. These results support the direct binding of **DC_AC50** to potential copper-transfer interfaces of the copper chaperones.

DC_AC50 reduces cancer cell proliferation and tumour growth

Further evaluation revealed that **DC_AC50** is highly efficient at inhibiting cancer cell proliferation (human lung cancer H1299 cells, leukaemia cancer K562 cells, breast cancer MDA-MB-231 cells and head and neck cancer 212LN cells) in a dose-dependent manner (Fig. 3a) with minimal effects on several non-cancerous cell lines (normal human immortalized melanocyte PIG1 cells, HDF cells and human immortal keratinocyte HaCaT cells) (Fig. 3b). In addition, we found that **DC_AC50** fails to exhibit any notable inhibition of the cell proliferation of human normal epithelial lung BEAS-2B cells or breast MCF-10A cells as control cells (Fig. 3b,c). Using western blotting, we confirmed that both Atox1 and CCS were expressed at higher levels in lung cancerous H1299 cells compared with normal cells (Supplementary Fig. 6a,b). To demonstrate that Atox1 and CCS are cellular targets of **DC_AC50**, we performed the knockdown of Atox1 or CCS in lung cancer H1299 cells by using short-hairpin RNA (Supplementary Fig. 6c), which resulted in a reduced cell proliferation (Fig. 3d), indicating that both proteins play important roles in cancer proliferation[22,27,28]. We further showed that re-expression of Atox1 and CCS rescued cell proliferation in the corresponding knockdown cells (Supplementary Fig. 7a,b). Importantly, we observed no significant decrease in cell proliferation of the Atox1/CCS knockdown normal HaCaT cells (Fig. 3e), which suggests Atox1 and CCS are of special importance for cancer cell proliferation compared with normal cell proliferation.

To examine further Atox1 and CCS as cellular targets of **DC_AC50**, we also tested ZYAT36, an inactive control compound that has a similar chemical structure to that of **DC_AC50** (Fig. 3f and the Supplementary Information), but does not bind tightly to Atox1 and CCS ($K_d > 250$ μM for Atox1 and ~118 μM for full-length CCS) (Supplementary Fig. 3g,h). We observed minimal effects of cell-proliferation inhibition in H1299 cells when using this compound (Fig. 3g). We also studied the inhibition of H1299 cells with a stable knockdown of either Atox1 or CCS, as well as a double knockdown. Cells with a stable knockdown of either Atox1 or CCS were still susceptible to the treatment with **DC_AC50**, but to a lesser extent compared with the control without knockdown; however, double knockdown of Atox1 and CCS resulted in a diminished further inhibition of cell proliferation by **DC_AC50** (Fig. 3h), and thus establishes Atox1 and CCS as cellular targets of **DC_AC50**. Finally, we performed a cellular thermal-shift assay, a recently developed target-engagement assay[29], to confirm the cellular binding of **DC_AC50** to both proteins

(Supplementary Fig. 7c,d). Taken together, these results support Atox1 and CCS as the cellular targets of **DC_AC50** in inhibiting cancer cell proliferation.

To test the effect of **DC_AC50** on tumour xenograft growth, we synthesized a large quantity of **DC_AC50** for animal model work (see the Supplementary Information). The initial toxicity studies by the chronic injection of **DC_AC50** (100 mg kg^{-1} per day) into nude mice revealed that **DC_AC50** did not result in significant alterations in complete blood-cell counts or in the haematopoietic properties of nude mice (Supplementary Fig. 8). Then, nude mice were injected with lung cancer H1299 cells (Fig. 3i and Supplementary Fig. 9a) or leukaemia cancer K562 cells (Supplementary Fig. 9b) and treated with 100 mg kg^{-1} per day of **DC_AC50** for 21 days. We found that treatment with **DC_AC50** resulted in a significantly decreased tumour size compared with mice that received the vehicle control. We lowered the dose to 10, 20 and 50 mg kg^{-1} per day, and found similar tumour-inhibition effects in the leukaemia K562 mice model (Supplementary Fig. 10a–c). At doses of 10–50 mg kg^{-1} per day, **DC_AC50** did not cause any obvious toxicity or a change in body weight or haematological properties in mice (Supplementary Fig. 10d,e). Next, a cellular thermal-shift assay was performed in tumour tissues isolated from H1299 nude xenograft mice, which revealed that the treatment with **DC_AC50** stabilized Atox1 and CCS in these tumour tissues at 10 mg kg^{-1} per day and 50 mg kg^{-1} per day (Supplementary Fig. 11a). These data indicate that targeting Atox1 and CCS by **DC_AC50** can suppress tumour growth effectively without affecting normal tissues in mice.

DC_AC50 induces cellular reactive oxygen species (ROS) accumulation

The high efficacy and selectivity against cancer cells and tumour xenograft by **DC_AC50** prompted us to investigate further the underlying mechanism with H1299 as a model cell line. We employed inductively coupled plasma mass spectrometry to measure the total cellular copper content on the inhibition of Atox1 and CCS in H1299 cells. The addition of **DC_AC50** led to an increase of ~45% in the total cellular copper content (Fig. 4a). As expected, we found that treatment with **DC_AC50** (10 mg kg^{-1} per day) induced a copper accumulation of ~20% in tumour tissues isolated from H1299 nude xenograft mice (Supplementary Fig. 11b). Atox1 is crucial for copper secretion; therefore, its inhibition is expected to increase the total cellular copper content[27] (an increase of ~53% was observed on Atox1 knockdown). The knockdown of CCS also led to a slight accumulation of cellular copper (~22%), which could be caused by the disruption of cellular copper trafficking. When we knocked down both Atox1 and CCS we observed another increase in cellular copper content (~73%) compared with the knockdown of just Atox1, in agreement with the results obtained when **DC_AC50** was used as an inhibitor (Fig. 4a). As a control, we added the copper chelator tetrathiomolybdate (TM), and observed a decrease of the total cellular copper content (~40%), as expected (Fig. 4a). Meanwhile, we observed increased levels of metallothionein 12 hours after **DC_AC50** treatment (Supplementary Fig. 12a). This effect could also result from the increased cellular copper level induced by **DC_AC50** treatment. We wondered whether cellular copper accumulation might contribute to oxidative stress. Indeed, we found that Atox1/CCS knockdown or the treatment of H1299 cells with **DC_AC50** (10 μM) led to a significant increase in cellular ROS levels (Fig. 4b,c), accompanied by a decrease in the reduced glutathione (GSH) level and an increase in the

oxidized glutathione (GSSG) level in H1299 cells (Fig. 4d,e). In contrast, the ROS level did not change in normal HaCaT cells with **DC_AC50** treatment or in H1299 cells with the inactive control compound ZYAT36 (Fig. 4f,g). We also noticed a moderate reduction in the ratio of nicotinamide adenine dinucleotide (NADPH)/NADP$^+$) in H1299 cancer cells after **DC_AC50** treatment or Atox1/CCS knockdown (Fig. 4h,i; see the next section (**DC_AC50** reduces cellular ATP production) for a mechanism that underlies reduced NADPH); NADPH provides the main reducing equivalents to counter the toxicity of ROS through the regeneration of GSH. The ROS increase observed in H1299 cells can be rescued almost completely by treatment with the ROS scavenger *N*-acetyl-L-cysteine (NAC) (Fig. 4j).

Next, we examined whether a change of cellular SOD activity may also contribute to the increased oxidative stress when the dysfunction of copper delivery from CCS to SOD1 occurs. We found that the total SOD activity increased at 12 hours, but decreased after 48 hours of treatment with **DC_AC50** in H1299 cells (Supplementary Fig. 12b). Meanwhile, we observed a fluctuation in the levels of the SOD1 and SOD2 in H1299 cells treated with **DC_AC50** (Supplementary Fig. 12c). Then, we examined the effect of **DC_AC50** on the activities of SOD1 and SOD2 by an ingel SOD-activity assay. Treatment with **DC_AC50** in H1299 cells resulted in increased activities at 12 hours, but in reduced activities after 48 hours for both proteins (Supplementary Fig. 12d), consistent with the reduced total SOD activity observed after 12 hours and 48 hours. The short-term elevation of total SOD activity could result from an adaptive response to increased ROS stress. However, the blockage of copper supply eventually led to a reduced total SOD activity after 48 hours. Finally, we tested the inactive control compound ZYAT36, which did not induce changes of the total SOD activity nor of the protein levels in H1299 cells (Supplementary Fig. 12e,f). Therefore, the reduced cellular SOD activity could also contribute to the increased ROS level on **DC_AC50** treatment.

The presence of an increased oxidative stress was confirmed by the observation of noticeably increased levels of 8-oxo-2′-deoxyguanosine (8-oxo-dG) in cancerous genomic DNA, one of the major products of DNA oxidation during oxidative damage after **DC_AC50** treatment or Atox1/CCS knockdown (Supplementary Fig. 13a,b). Importantly, **DC_AC50** did not lead to an obvious increase in the 8-oxo-dG level in normal HaCaT cells (Supplementary Fig. 13c). Interestingly, treatment with **DC_AC50** did not noticeably induce apoptosis in H1299 cancer cells and in normal cells (HaCaT and MCF-10A) (Supplementary Fig. 14). As redox balancing is much more sensitive to cancer cell survival[30,31] compared with that of normal cells, the selective inhibition of cancer cell proliferation could be achieved with **DC_AC50** by inducing ROS specifically in cancer cells, leaving normal cell proliferation unaffected.

DC_AC50 reduces cellular ATP production

Metabolic processes play an essential role in the regulation of the cellular redox balance. Prior research shows that high levels of ROS can lead to mitochondrial dysfunction[32]. To establish if the inhibition of copper trafficking results in additional metabolic defects in cancer cells, we examined the bioenergetics properties of **DC_AC50**-treated cells. Aerobic glycolysis is a key metabolic character in various human cancers[33–35]. However, although

we observed noticeably reduced cellular ATP levels on treatment with **DC_AC50** or Atox1/CCS knockdown in H1299 cells (Fig. 5a), neither treatment significantly altered lactate production, glucose uptake or glycolytic rate (Supplementary Fig. 15a–d), which indicates that **DC_AC50** is unlikely to function directly within the glycolysis pathway.

Copper is also an essential cofactor for the electron-transfer and oxygen-reduction activity of cytochrome c oxidase (COX), the key enzyme responsible for oxygen reduction in the process of oxidative phosphorylation (OXPHOS) in mitochondria. This process provides energy for the aerobic metabolism of all animals, plants, yeasts and some bacteria. It is plausible that treatment with **DC_AC50** may result in the interference of OXPHOS, which would subsequently lead to an increased ROS level and reduced ATP production in these cancer cells.

Although proteins (for example, COX17) or potential copper ligands[2,36] may function in the copper delivery to COX, the exact mechanism as to how copper makes its way from the site of transport via Ctr1 to the mitochondrial intermembrane space in cancer cells is not well understood. Previous reports indicated that a defected ATP7B, one of the major copper-delivery targets of Atox1, could lead to altered COX activity in mice[37]. We found that the activities of COX (units ml^{-1}) in H1299 cells in the presence of **DC_AC50** are significantly lower than those of the control (Fig. 5b). To investigate further the potential effects of Atox1 and CCS on COX activities, we knocked down Atox1 and CCS in H1299 cells, and observed decreased COX activities as found in the experiment with **DC_AC50** treatment (Fig. 5c). We also showed that re-expression of Atox1 and CCS rescued COX activity in H1299 cells in the presence of **DC_AC50** (Fig. 5d). This result strongly indicates that **DC_AC50** influences COX activity through Atox1 and CCS in these cells. Next, after **DC_AC50** treatment or Atox1/CCS knockdown we observed a reduced expression of COX sububits 1 and 2 (COX1 and COX2) (Fig. 5e,f), which are two copper-binding sub-units of COX. Treatment with **DC_AC50** or Atox1/CCS knockdown resulted in significant decreases in the rate of oxygen consumption (Fig. 5g,h) and reduced NADH level (Supplementary Fig. 15e–g) in H1299 cells. As expected, the inactive control compound ZYAT36 caused minimal effects on the ATP level, COX activities and oxygen consumption in the same H1299 cells (Fig. 5i–l).

DC_AC50 decreases lipid biosynthesis through AMP-activated protein kinase (AMPK) activation

To maintain a normal cellular ATP level is critical to cancer cell proliferation[33,35]. A defective OXPHOS may preferentially signal the inhibition of growth in cancer cells. Indeed, although **DC_AC50** treatment did not affect glucose-dependent RNA synthesis (Supplementary Fig. 15h), we observed significant decreases in lipid biosynthesis and the NADPH/NADP$^+$ ratio in the H1299 cancer cells (Figs 4h and 6a,b). These data are consistent with our observation that **DC_AC50** does not affect glycolysis but rather inhibits mitochondrial OXPHOS, because RNA biosynthesis depends on glycolytic intermediates derived from the pentose phosphate pathway (PPP), whereas lipid biosynthesis makes use of citrate from the tricarboxylic acid cycle and NADPH as precursors. NADPH is the most crucial metabolite produced by the PPP; NADPH not only fuels lipid biosynthesis, but also

functions as a crucial antioxidant, quenching ROS produced during the rapid proliferation of cancer cells. The reduced NADPH production observed with **DC_AC50** treatment in cancer cells should potentiate ROS accumulation further.

To elucidate in more detail the mechanism that underlies the **DC_AC50**-dependent inhibition of lipogenesis, we reasoned that reduced levels of ATP would result in the activation of the AMP-activated protein kinase[38,39], a central sensor of cellular metabolism, which subsequently leads to increased phosphorylation of its direct target, acetyl-CoA carboxylase 1 (ACC1), and the inhibition of lipid biosynthesis[40,41]. Indeed, treatment with **DC_AC50** increased the levels of AMPK phosphorylation (p-AMPK) and ACC1 phosphorylation (p-ACC1) (Fig. 6c). In our subsequent investigations we observed significantly reduced lipid biosynthesis in H1299 cancer cells with Atox1 and/or CCS knockdown (Fig. 6d,e). The effects are less significant in the non-cancer HaCaT cell line or with the use of an inactive control compound ZYAT36 (Fig. 6f-h). The ROS scavenger NAC failed to rescue these effects; however, treatment with an AMPK inhibitor compound C together with **DC_AC50** almost completely reversed the increased phosphorylation on both proteins, and recovered lipid biosynthesis in H1299 cells (Fig. 6i). Together these data indicate that the inhibition of copper trafficking by **DC_AC50** results in metabolic attenuations in bioenergetics (OXPHOS), anabolic biosynthesis (lipogenesis) and redox homeostasis (ROS production), which all lead to the preferential inhibition of cancer cell proliferation.

We next sought to determine if the combination of these effects could account for the observed inhibition of cancer cell proliferation by **DC_AC50**, or if any were cellular responses to a decreased cancer cell proliferation. We found that treatment with either NAC or compound C partially rescued the cancer cell proliferation caused by **DC_AC50** (Fig. 6j). When cells were treated with both NAC and compound C, we observed an almost complete rescue of cell-proliferation inhibition induced by **DC_AC50** (Fig. 6j). These results further support that the inhibition of copper trafficking induces an increased ROS level and AMPK activation (through a reduced ATP production), which together attenuate cancer cell proliferation and tumour growth. The combined results presented here also establish Atox1 and CCS as viable anticancer targets and copper trafficking as a new pathway for future therapeutic developments.

Discussion

Copper plays essential roles in mammalian bioenergetics and is critical in controlling cellular ROS levels; both processes are crucial to cancer cell proliferation[42–45]. Cancer cells are known to accumulate more copper than normal cells. To deplete cellular copper, copper chelators, such as TM, were developed previously to study cell responses under copper 'starvation' conditions[46,47]. Although the information gained in this regard has been valuable, these chelators suffer from the nonspecific binding of copper and other metal ions, which depletes both intracellular and extracellular copper, and thus leads to toxicity effects. We report here small molecules that specifically block copper-transport proteins inside cells without depleting the extracellular copper, which allows for the investigation of the precise cellular effects as well as the underlying mechanisms associated with the selective inhibition of copper trafficking.

With the small molecules that we developed to block the copper-trafficking chaperones Atox1 and CCS, we observed the selective inhibition of cancer cell proliferation with minimal effects on normal cells at the doses we applied. Mouse-model experiments further confirmed the effective inhibition of tumour growth with minimum side effects observed. The inhibitor leads to an accumulation of cellular copper instead of the depletion typically observed with the use of copper chelators.

By using cell-proliferation assays with H1299 (lung cancer), K562 (leukaemia), MB231 (breast cancer) and 212LN (head and neck cancer), we showed that treatment with **DC_AC50** markedly reduced cell proliferation in these human cancer cell lines. We noticed significantly increased ROS levels in these cells, but not in normal cells, on treatment with **DC_AC50**. Several effects could contribute to the increased cellular ROS level: (1) the overall accumulation of copper inside the cells and the decreased SOD1 activity on blocking Atox1 and CCS (Fig. 4a and Supplementary Fig. 12d) increase oxidative stress; (2) the reduced ATP production leads to reduced cellular NADPH and GSH, which are critical for the elimination of ROS produced in cancer cells. GSH was recently suggested to play an important role in copper and copper-chaperone interactions[48]; the reduced GSH level may also affect copper uptake in mammalian cells. The combination of these effects could give rise to significantly increased ROS levels in cancer cells on blocking copper chaperones with **DC_AC50** (Supplementary Fig. 17). As cancer cells produce more ROS[42–44] and are more sensitive to ROS[30,31], a preferential inhibition of cancer cell proliferation on inhibiting Atox1 and CCS occurred. An inactive control compound does not induce ROS accumulation and fails to inhibit cell proliferation.

We have also shown that the activity of COX is reduced on the knockdown of Atox1 and CCS or inhibition of these proteins using the inhibitor in cancer cells. This result suggests that Atox1 and CCS may directly or indirectly contribute to copper trafficking across mitochondrial membranes in cancer cells. The attenuated OXPHOS, most probably the result of insufficient copper transport to COX, leads to decreased ATP production and activation of AMPK, which subsequently leads to increased phosphorylation of the direct targets of AMPK and ACC1, and probably to inhibition of lipid biosynthesis. It is possible that additional pathways exist to connect cellular copper availability to lipid metabolisms, which may also explain the observed effects through inhibiting the copper delivery inside cancer cells. Again, an inactive control compound fails to elicit these effects. A recent study also showed that the administration of the copper chelator TM leads to a reduced copper loading to COX and tumour-growth inhibition[46].

Lastly, the **DC_AC50**-based inhibition reduced cell proliferation as potently as cisplatin and more effectively than the copper chelator TM (Supplementary Fig. 16). The use of TM to disrupt copper loading to COX could reduce ATP production and limit tumour growth[46]. However, increased ROS was not observed using a copper chelator. The increased glycolytic activity with the use of a copper chelator was not observed in our approach. We show here that by specifically targeting copper-transport proteins Atox1 and CCS with small molecules, we can generate decreased lipogenesis via reduced ATP production and significantly increase the ROS levels. Both effects contribute to a specific and significant inhibition of cancer cell proliferation (Supplementary Fig. 17).

Our inhibitor targets the protein–protein interaction interface of Atox1 and potential copper-trafficking surface on CCS, and exhibits low micromolar affinities to Atox1 and CCS. Although we have multiple experiments to demonstrate both *in vitro* and *in vivo* effects of the inhibitor, we could not exclude the potential presence of other targets that may work synergistically with the inhibition of Atox1 and CCS. However, the cell-proliferation inhibition demonstrated through the knockdown of both copper chaperones establishes these proteins as potential new targets for future anticancer biomedical research and therapeutic developments. The inhibitor and strategy presented here should stimulate future research and developments towards this goal.

Methods

Virtual screening for Atox1-binding small molecules

A hierarchical virtual-screening strategy was based on characterized structures and the established copper-transfer mechanism[11–14]. DOCK4.0 was used for the initial screening on the Specs database, which contains more than 200,000 commercially available compounds. The Atox1 crystal structure (PDB entry 1FEE) was used as the docking receptor and residues in the copper-transfer protein–protein interaction interface were defined as the binding site. A standard DOCK scoring function was used to rank the result list and the top-ranked 10,125 candidates were rescored by the CSCORE (consensus score) module of SYBYL 6.8 (Tripos Inc.). CSCORE combines multiple types of scoring functions, including FlexX, Dock, Gold, ChemScore and Potential Mean Force scoring schemes to produce a consensus to evaluate ligand– receptor interactions.

Compounds that had a consensus score of four or five or that were ranked in the top 10% by at least four out of five scoring functions were evaluated further by Autodock 4.0[49]. Based on an empirical binding free energy estimated by Autodock 4.0, 301 compounds with the highest estimated binding affinity were chosen, and then structurally clustered to 50 clusters based on their two-dimensional (2D) molecular fingerprints using the Cluster Molecules module in Pipeline Pilot 7.5 (Scitegic, Inc.). To ensure the structural diversity of the selected compounds, two to three compounds with good drug-like properties (molecular weight <500, log P < 5 and polar surface area <140 Å) were selected from each cluster. Finally, 127 compounds in total were selected and purchased for the first round of biochemical assay described below. Based on the structures of the four active compounds identified by the first-round biochemical assay, a 2D similarity search and scaffold hopping were conducted using FP2 and SHAFTS methods implemented in the ChemMapper web server[50]. After water-solubility prediction and structural clustering of the 520 newly screened hits using Solubility and Cluster Molecules modules implemented in Pipeline Pilot 7.5, 110 structurally diverse candidates were purchased for the final biochemical assay.

eCALWY3 FRET measurement

FRET with eCALWY3 (1 μM) was performed in 150 mM HEPES, 100 mM NaCl, 1 mM dithiothreitol (DTT) and 10% glycerol (pH 7.1). Zn^{2+} titration was performed by mixing 0.9 mM Zn^{2+} from a slightly acidic stock solution of $ZnCl_2$ with buffering systems that consisted of 1 mM DHPTA (1,3-diaminopropanol tetraacetic acid). Subsequently, we treated

the FRET probe with 100 μM of the small molecules identified from the computational screen. The volume of dimethylsulfoxide (DMSO) was less than 5 μl in 200 μl HEPES buffer. Fluorescence spectra were recorded on a Varian Cary Eclipse spectrometer. Protein concentration was determined by measuring the citrine absorbance at 515 nm using an extinction coefficient of 77,000 M^{-1} cm^{-1}. The eCALWY3 excitation is at 433 nm and the citrine/cerulean emission ratio was calculated by dividing the emissions at 527 nm and 475 nm, respectively.

Measurement of ROS production

Cells were treated with DMSO and **DC_AC50** for 12 hours and ROS generation was detected with dichlorodihydrofluorescein diacetate (DCFH-DA). Cells were incubated with 10 μM DCFH-DA for 30 minutes at 37 °C, washed twice with PBS and immediately analysed with a FACScan flow cytometer. H1299 cells were treated with 3 mM NAC and 5 μM **DC_AC50** for 12 hours. Results are represented as the mean and s.e.m. of at least three independent experiments.

Measurement of intracellular ATP production

An ATP-bioluminescent somatic-cell assay kit (Sigma) was used to measure the intracellular ATP concentration. Cells were treated with DMSO and **DC_AC50** for 12 hours and 1×10^6 cells were trypsinized and resuspended in ultrapure water. Luminescence was measured with a spectrofluorometer (SPECTRA Max Gemini, Molecular Probe) immediately after the addition of the ATP enzyme mix to the cell suspension. The results are represented as the mean and s.e.m. of at least three independent experiments.

Supplementary Material

Refer to Web version on PubMed Central for supplementary material.

Acknowledgments

References

1. Labbe S, Thiele DJ. Pipes and wiring: the regulation of copper uptake and distribution in yeast. Trends Microbiol. 1999; 7:500–505. [PubMed: 10603486]

2. Kim BE, Nevitt T, Thiele DJ. Mechanisms for copper acquisition, distribution and regulation. Nature Chem Biol. 2008; 4:176–185. [PubMed: 18277979]

3. O'Halloran TV, Culotta VC. Metallochaperones, an intracellular shuttle service for metal ions. J Biol Chem. 2000; 275:25057–25060. [PubMed: 10816601]

4. Rosenzweig AC. Copper delivery by metallochaperone proteins. Acc Chem Res. 2001; 34:119–128. [PubMed: 11263870]

5. Lutsenko S, Gupta A, Burkhead JL, Zuzel V. Cellular multitasking: the dual role of human Cu-ATPases in cofactor delivery and intracellular copper balance. Arch Biochem Biophys. 2008; 476:22–32. [PubMed: 18534184]

6. La Fontaine S, Mercer JF. Trafficking of the copper-ATPases, ATP7A and ATP7B: role in copper homeostasis. Arch Biochem Biophys. 2007; 463:149–167. [PubMed: 17531189]

7. Rae TD, Schmidt PJ, Pufahl RA, Culotta VC, O'Halloran TV. Undetectable intracellular free copper: the requirement of a copper chaperone for superoxide dismutase. Science. 1999; 284:805–808. [PubMed: 10221913]

8. Banci L, et al. Human superoxide dismutase 1 (hSOD1) maturation through interaction with human copper chaperone for SOD1 (hCCS). Proc Natl Acad Sci USA. 2012; 109:13555–13560. [PubMed: 22869735]

9. Caruano-Yzermans AL, et al. Mechanisms of the copper-dependent turnover of the copper chaperone for superoxide dismutase. J Biol Chem. 2006; 281:13581–13587. [PubMed: 16531609]

10. Rae TD, et al. Mechanism of Cu,Zn-superoxide dismutase activation by the human metallochaperone hCCS. J Biol Chem. 2001; 276:5166–5176. [PubMed: 11018045]

11. Lamb AL, et al. Crystal structure of the copper chaperone for superoxide dismutase. Nature Struct Biol. 1999; 6:724–729. [PubMed: 10426947]

12. Wernimont AK, Huffman DL, Lamb AL, O'Halloran TV, Rosenzweig AC. Structural basis for copper transfer by the metallochaperone for the Menkes/Wilson disease proteins. Nature Struct Biol. 2000; 7:766–771. [PubMed: 10966647]

13. Anastassopoulou I, et al. Solution structure of the apo and copper(I)-loaded human metallochaperone HAH1. Biochemistry. 2004; 43:13046–13053. [PubMed: 15476398]

14. Lamb AL, Torres AS, O'Halloran TV, Rosenzweig AC. Heterodimeric structure of superoxide dismutase in complex with its metallochaperone. Nature Struct Biol. 2001; 8:751–755. [PubMed: 11524675]

15. Kawamata H, Manfredi G. Different regulation of wild-type and mutant Cu, Zn superoxide dismutase localization in mammalian mitochondria. Hum Mol Genet. 2008; 17:3303–3317. [PubMed: 18703498]

16. Valentine JS, Hart PJ. Misfolded CuZnSOD and amyotrophic lateral sclerosis. Proc Natl Acad Sci USA. 2003; 100:3617–622. [PubMed: 12655070]

17. Mandinov L, et al. Copper chelation represses the vascular response to injury. Proc Natl Acad Sci USA. 2003; 100:6700–6705. [PubMed: 12754378]

18. Eatock MM, Schatzlein A, Kaye SB. Tumour vasculature as a target for anticancer therapy. Cancer Treat Rev. 2000; 26:191–204. [PubMed: 10814561]

19. Lowndes SA, Harris AL. The role of copper in tumour angiogenesis. J Mammary Gland Biol Neoplasia. 2005; 10:299–310. [PubMed: 16924372]

20. Folkman J. Angiogenesis in cancer, vascular, rheumatoid and other disease. Nature Med. 1995; 1:27–31. [PubMed: 7584949]

21. Gupte A, Mumper RJ. Elevated copper and oxidative stress in cancer cells as a target for cancer treatment. Cancer Treat Rev. 2009; 35:32–46. [PubMed: 18774652]

22. Cai H, Peng F. Knockdown of copper chaperone antioxidant-1 by RNA interference inhibits copper-stimulated proliferation of non-small cell lung carcinoma cells. Oncol Rep. 2013; 30:269–275. [PubMed: 23624903]

23. Boal AK, Rosenzweig AC. Structural biology of copper trafficking. Chem Rev. 2009; 109:4760–4779. [PubMed: 19824702]

24. Lutsenko S. Human copper homeostasis: a network of interconnected pathways. Curr Opin Chem Biol. 2010; 14:211–217. [PubMed: 20117961]

25. Wing TJ, Makino S, Skillman AG, Kuntz ID. DOCK 4.0: search strategies for automated molecular docking of flexible molecule databases. J Comput Aided Mol Des. 2001; 15:411–428. [PubMed: 11394736]

26. Vinkenborg JL, et al. Genetically encoded FRET sensors to monitor intracellular Zn^{2+} homeostasis. Nature Methods. 2009; 6:737–740. [PubMed: 19718032]

27. Hamza I, et al. The metallochaperone Atox1 plays a critical role in perinatal copper homeostasis. Proc Natl Acad Sci USA. 2001; 98:6848–6852. [PubMed: 11391006]

28. Itoh S, et al. Novel role of antioxidant-1 (Atox1) as a copper-dependent transcription factor involved in cell proliferation. J Biol Chem. 2008; 283:9157–9167. [PubMed: 18245776]

29. Martinez Molina D, et al. Monitoring drug target engagement in cells and tissues using the cellular thermal shift assay. Science. 2013; 341:84–87. [PubMed: 23828940]

30. Gad H, et al. MTH1 inhibition eradicates cancer by preventing sanitation of the dNTP pool. Nature. 2014; 508:215–221. [PubMed: 24695224]

31. Huber KV, et al. Stereospecific targeting of MTH1 by (S)-crizotinib as an anticancer strategy. Nature. 2014; 508:222–227. [PubMed: 24695225]

32. Sena LA, Chandel NS. Physiological roles of mitochondrial reactive oxygen species. Mol Cell. 2012; 48:158–167. [PubMed: 23102266]

33. Kroemer G, Pouyssegur J. Tumor cell metabolism: cancer's Achilles' heel. Cancer Cell. 2008; 13:472–482. [PubMed: 18538731]

34. Vander Heiden MG, Cantley LC, Thompson CB. Understanding the Warburg effect: the metabolic requirements of cell proliferation. Science. 2009; 324:1029–1033. [PubMed: 19460998]

35. Cairns RA, Harris IS, Mak TW. Regulation of cancer cell metabolism. Nature Rev Cancer. 2011; 11:85–95. [PubMed: 21258394]

36. Leary SC, et al. 'Pulling the plug' on cellular copper: the role of mitochondria in copper export. Biochim Biophys Acta. 2009; 1793:146–153. [PubMed: 18522804]

37. Sauer SW, et al. Severe dysfunction of respiratory chain and cholesterol metabolism in Atp7b(-/-) mice as a model for Wilson disease. Biochim Biophys Acta. 2011; 1812:1607–1615. [PubMed: 21920437]

38. Mihaylova MM, Shaw RJ. The AMPK signalling pathway coordinates cell growth, autophagy and metabolism. Nature Cell Biol. 2011; 13:1016–1023. [PubMed: 21892142]

39. Hardie DG, Ross FA, Hawley SA. AMPK: a nutrient and energy sensor that maintains energy homeostasis. Nature Rev Mol Cell Biol. 2012; 13:251–262. [PubMed: 22436748]

40. Carracedo A, Cantley LC, Pandolfi PP. Cancer metabolism: fatty acid oxidation in the limelight. Nature Rev Cancer. 2013; 13:227–232. [PubMed: 23446547]

41. Schulze A, Harris AL. How cancer metabolism is tuned for proliferation and vulnerable to disruption. Nature. 2012; 491:364–373. [PubMed: 23151579]

42. Trachootham D, Alexandre J, Huang P. Targeting cancer cells by ROS-mediated mechanisms: a radical therapeutic approach? Nature Rev Drug Discov. 2009; 8:579–591. [PubMed: 19478820]

43. Raj L, et al. Selective killing of cancer cells by a small molecule targeting the stress response to ROS. Nature. 2011; 475:231–234. [PubMed: 21753854]

44. Gorrini C, Harris IS, Mak TW. Modulation of oxidative stress as an anticancer strategy. Nature Rev Drug Discov. 2013; 12:931–947. [PubMed: 24287781]

45. Brady DC, et al. Copper is required for oncogenic BRAF signalling and tumorigenesis. Nature. 2014; 509:492–496. [PubMed: 24717435]

46. Ishida S, et al. Bioavailable copper modulates oxidative phosphorylation and growth of tumors. Proc Natl Acad Sci USA. 2013; 110:19507–19512. [PubMed: 24218578]

47. Santini C, et al. Advances in copper complexes as anticancer agents. Chem Rev. 2013; 114:815–862. [PubMed: 24102434]

48. Maryon EB, et al. Cellular glutathione plays a key role in copper uptake mediated by human copper transporter 1. Am J Physiol Cell Physiol. 2013; 304:C768–C779. [PubMed: 23426973]

49. Morris GM, et al. AutoDock4 and AutoDockTools4: automated docking with selective receptor flexibility. J Comput Chem. 2009; 30:2785–2791. [PubMed: 19399780]

50. Gong J, et al. ChemMapper: a versatile web server for exploring pharmacology and chemical structure association based on molecular 3D similarity method. Bioinformatics. 2013; 29:1827–1829. [PubMed: 23712658]
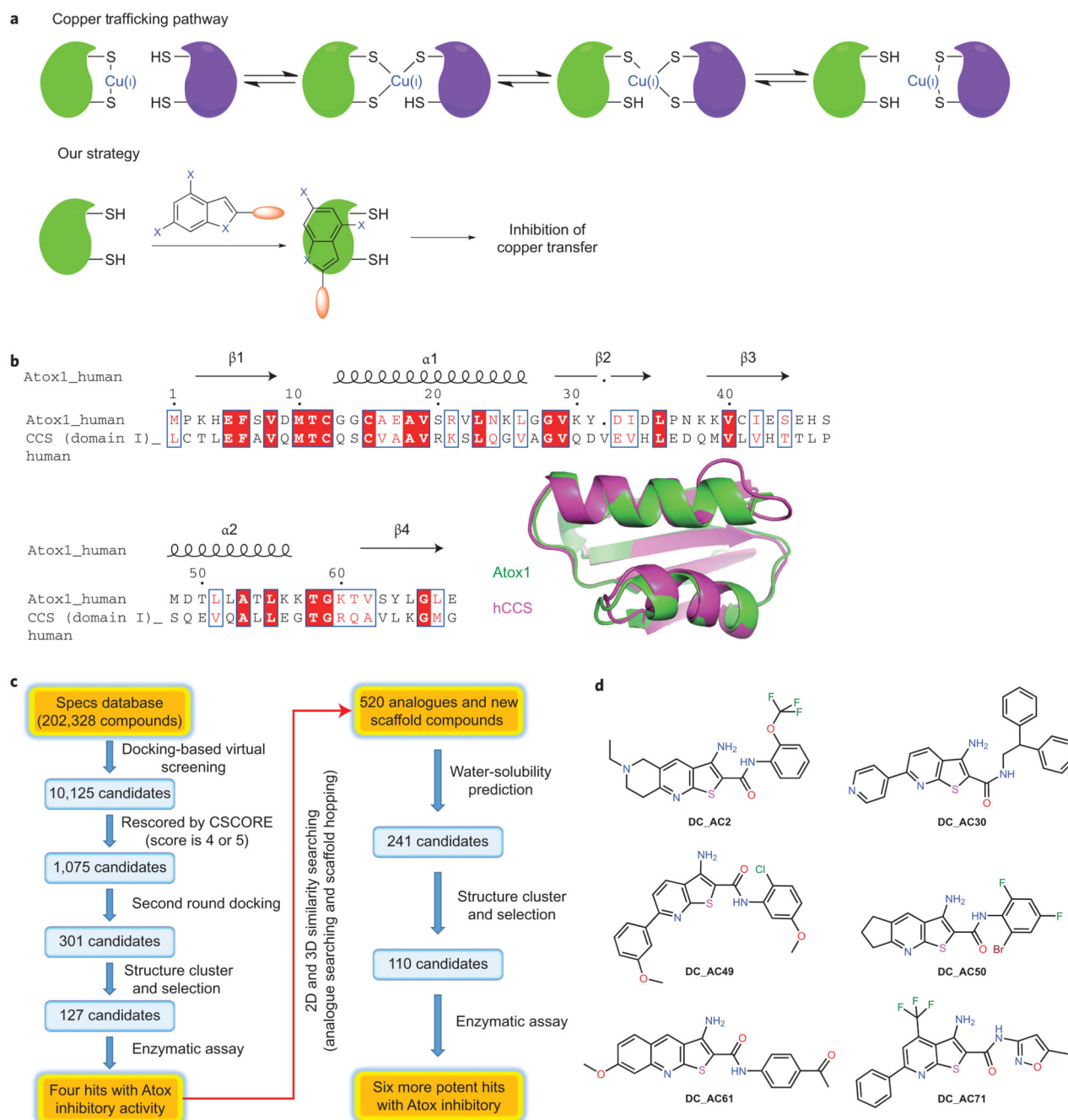
Figure 1. Developing small molecules that specifically inhibit human copper-trafficking proteins and an overview of the screening process

a, Copper trafficking in eukaryotes and the selective inhibition of human copper trafficking by a small molecule (**DC_AC50**). Green represents the copper chaperone proteins and lilac represents proteins that receive copper from the chaperones. **b**, The sequence alignment illustrates a significant similarity between human Atox1 and domain I of CCS. Structural comparison of human Atox1 (green; Protein Data Bank (PDB) 1TL4) and domain I of human CCS (hCCS, purple; PDB 2CRL). **c**, A hierarchical docking strategy was adopted:

DOCK4.0 was used to screen the Specs database, which contains more than 200,000 compounds. Out of this screen, and based on their structural features, physical chemistry properties and drug-like characteristics, 237 compounds were selected for further bioactivity testing with six hits discovered. **d**, The structures of the six representative hits.
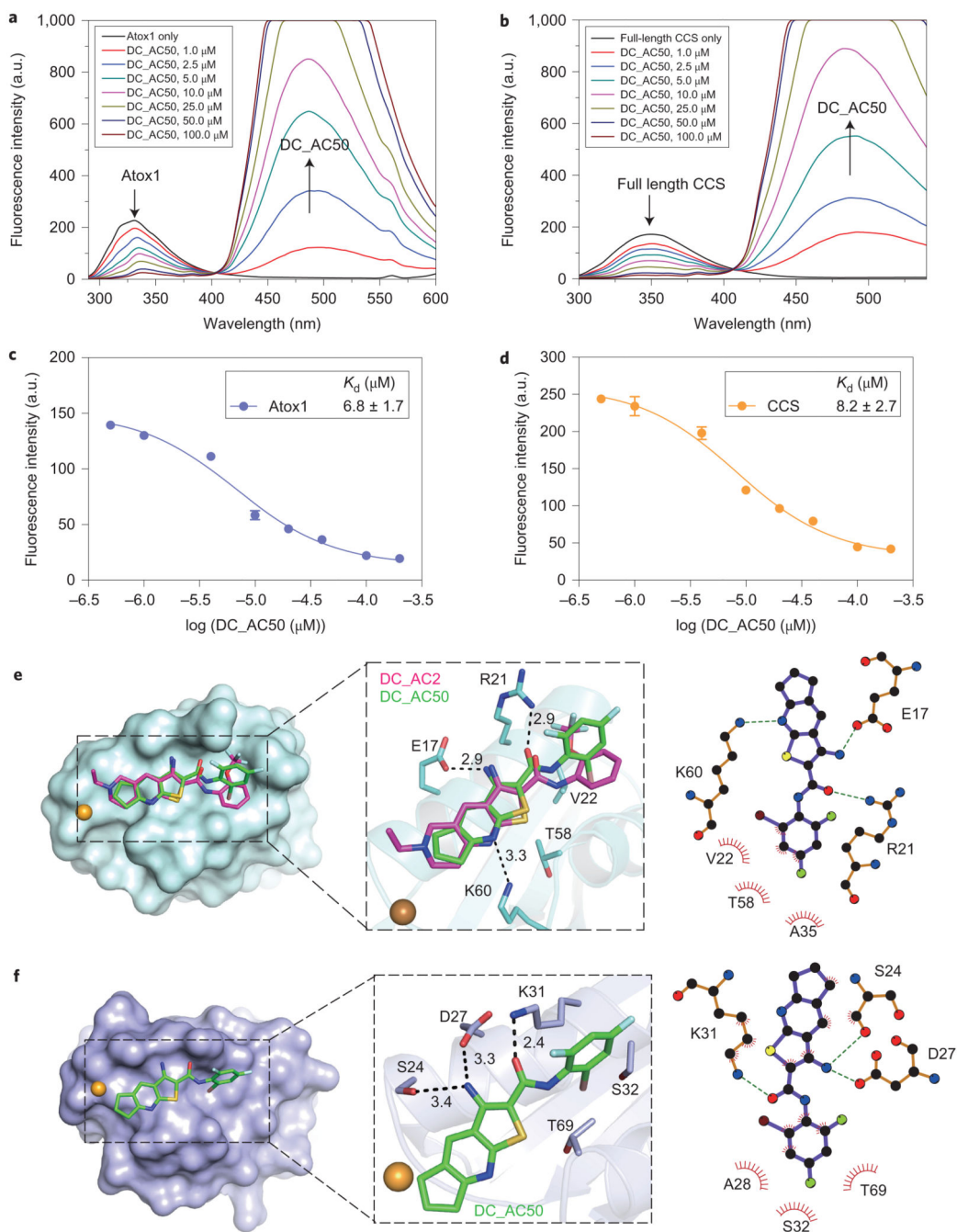
Figure 2. Docking model and binding of DC_AC50 to Atox1 and full-length CCS by FRET measurements (from Tyr/Trp to DC_AC50)

a,b, FRET between Atox1 (Tyr), full-length CCS (Trp) and **DC_AC50**. Atox1 or full-length CCS (1 μM) displayed the maximum fluorescence emission at 335 or 350 nm, respectively, in the absence of **DC_AC50**. With the addition of **DC_AC50** (1-100 μM and less than 5 μl DMSO in 200 μl buffer), the peak at 335 or 350 nm, which corresponds to the emission of Tyr or Trp, respectively, was reduced, whereas the emission of **DC_AC50** at 494 nm was increased. FRET changes are shown in coloured lines. **c,d,** Binding curves of **DC_AC50** to

Atox1 and CCS. The experiments were performed in 50 mM HEPES, 200 mM NaCl, 1 mM DTT (pH 7.1). **e,f,** Surface representations that show **DC_AC50** (green) and **DC_AC2** (purple) binding to Atox1 (**e**; PDB 1TL4) and CCS (**f**; PDB 2CRL). Error bars, mean ± s.e.m., n = 3 biological replicates.
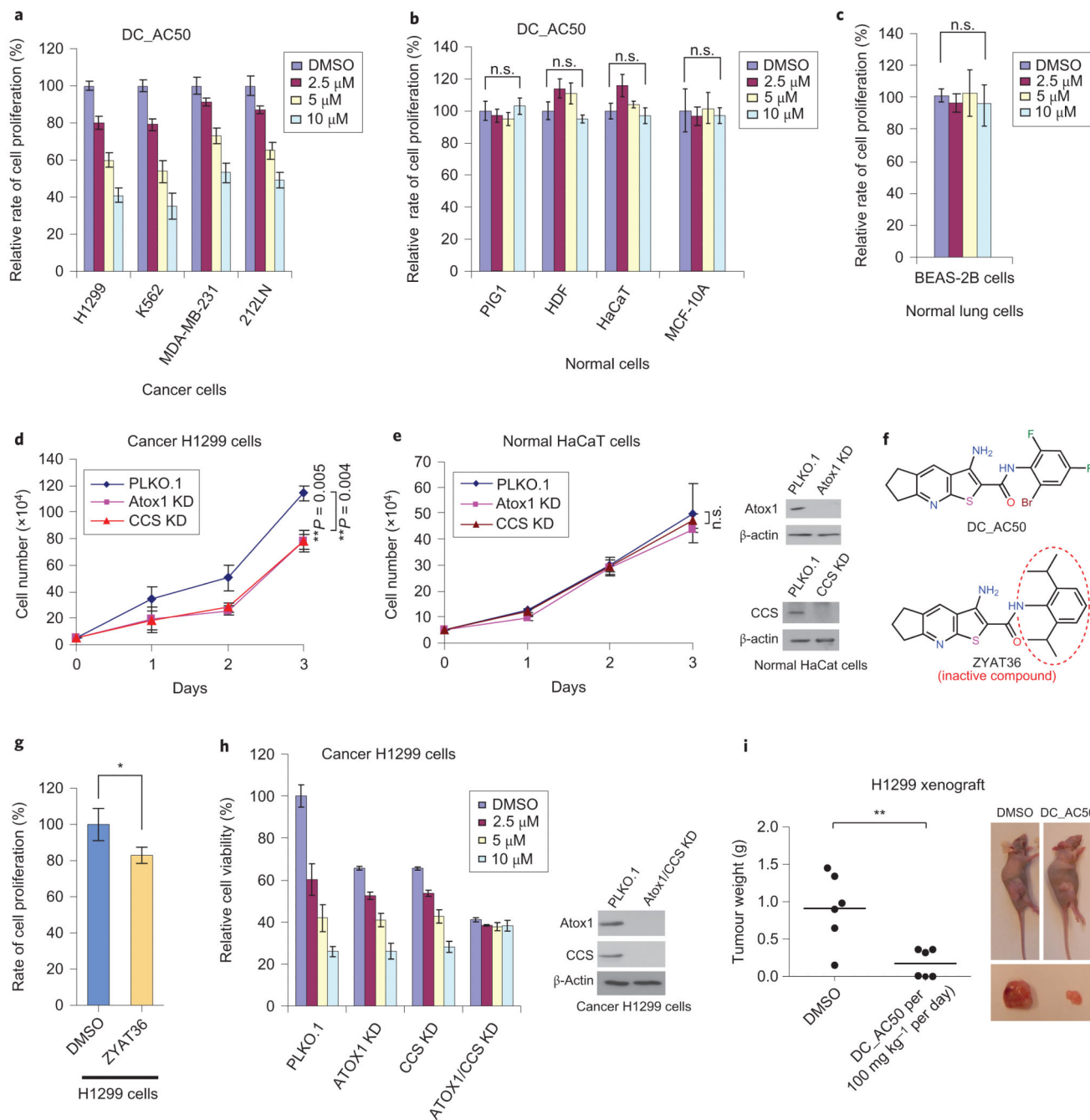
Figure 3. DC_AC50 reduces the proliferation of cancer cells and attenuates tumour growth in xenograft nude mice

a,b, Treatment with **DC_AC50** inhibits cancer cell proliferation (**a**) but not normal cell proliferation (**b**). Cells were grown and treated with **DC_AC50** at 0-10 μM for 72 hours. **c**, Cell proliferation of normal lung BEAS-2B cells showed minimal effects with **DC_AC50** (0-10 μM) treatment for 72 hours. **d**, Reduced cell proliferation on the knockdown (KD) of Atox1 and CCS. Knockdowns of Atox1 and CCS were confirmed via western blotting (Supplementary Fig. 7c). **e**, Knockdowns of Atox1 and CCS did not significantly reduce cell

proliferation in normal HaCaT cells. Knockdowns of Atox1 and CCS were confirmed via western blotting. **f**, The structures of **DC_AC50** and the inactive control compound ZYAT36. **g**, Treatment with the inactive control compound ZYAT36 at 10 μM showed minimal effects in the H1299 cells for 72 hours. **h**, Knockdowns of Atox1 and CCS resulted in a diminished further inhibition of cell proliferation by **DC_AC50** (0-10 μM). **i**, Tumour growth and tumour size in xenograft nude mice injected with H1299 cells compared with the group of mice treated with **DC_AC50** and the control group treated with vehicle control. PLKO.1 is the name of the lentiviral vector as a control for the stable knockdown assay. Error bars, mean ± s.e.m., $n = 3$ biological replicates. P values were determined by a two-tailed Student's t test. $*P < 0.05$, $**P < 0.005$. n.s., not significant.
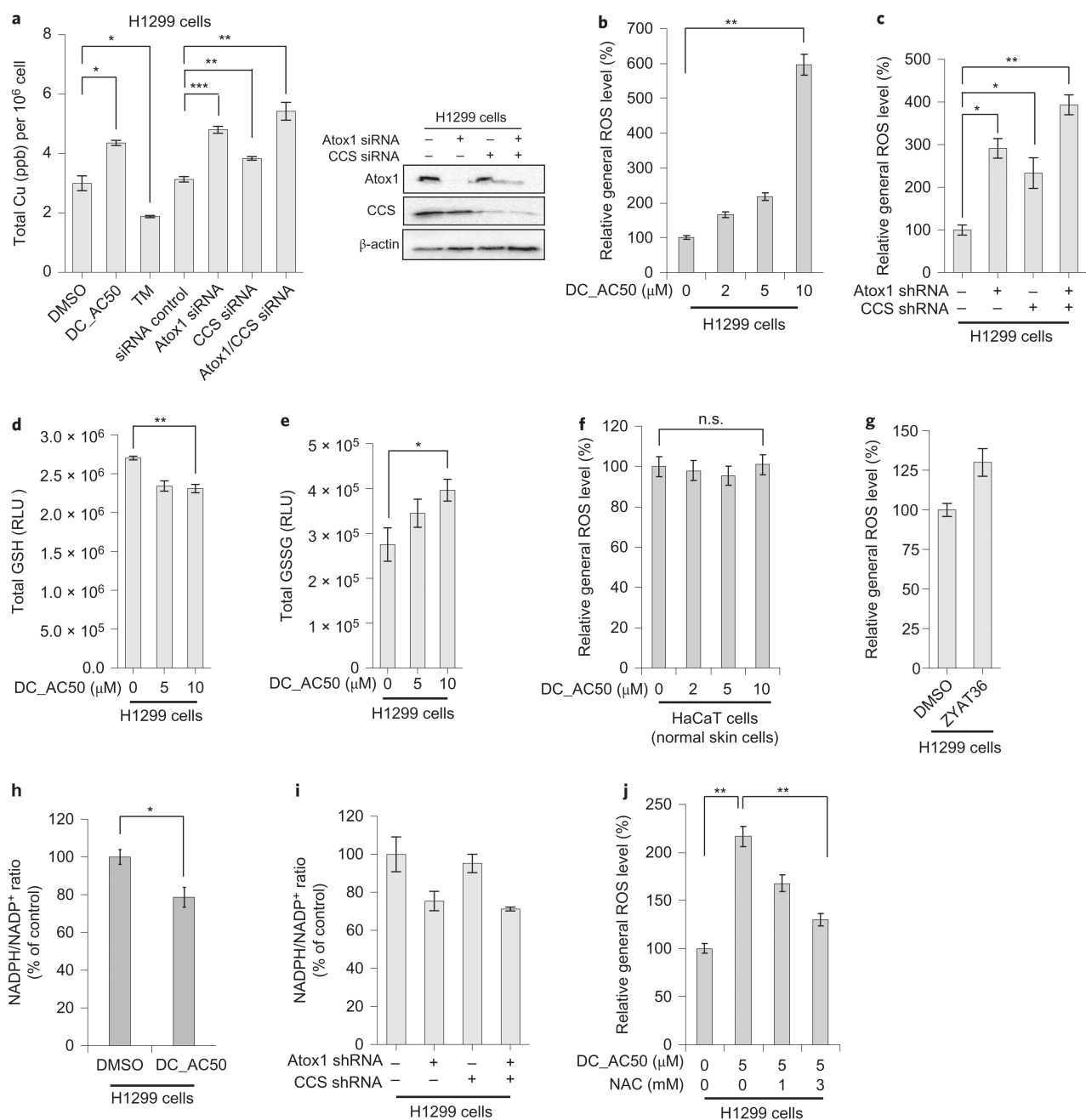
Figure 4. DC_AC50 induces copper accumulation, increases ROS level and decreases the NADPH/NADP⁺ ratio

a, The addition of **DC_AC50** (10 μM) and the knockdown of Atox1 both led to an increase in the total cellular copper after 12 hours. The knockdown of CCS also led to a slight increase in the cellular total copper content after 12 hours. Knockdowns of Atox1 and CCS were confirmed via western blotting. **b,c**, Treatment with **DC_AC50** or knockdown of Atox1/CCS induced ROS elevation in H1299 cells. **d,e**, **DC_AC50**-induced ROS elevation accompanied by a reduced total GSH and increased GSSG level in H1299 cells after 12 hours of treatment. **f,g**, The ROS levels showed minimal effects in normal HaCaT cells with

DC_AC50 treatment (0-10 μM) or in H1299 cells with the inactive control compound ZYAT36 (10 μM) treatment for 12 hours. **h,i**, The NADPH/NADP$^+$ ratio decreased with the **DC_AC50** treatment (10 μM) or Atox1/CCS knockdown in H1299 cells. **j**, **DC_AC50**-induced ROS can be rescued by NAC in H1299 cells. Cells were pretreated with 1 mM or 3 mM NAC for one hour, followed by 5 μM **DC_AC50** for 12 hours. Error bars, mean ± s.e.m., n = 3 biological replicates. *P < 0.05, **P < 0.005, ***P < 0.0005. RLU, relative luminescence units. shRNA, short hairpin RNA; siRNA, small interfering RNA.
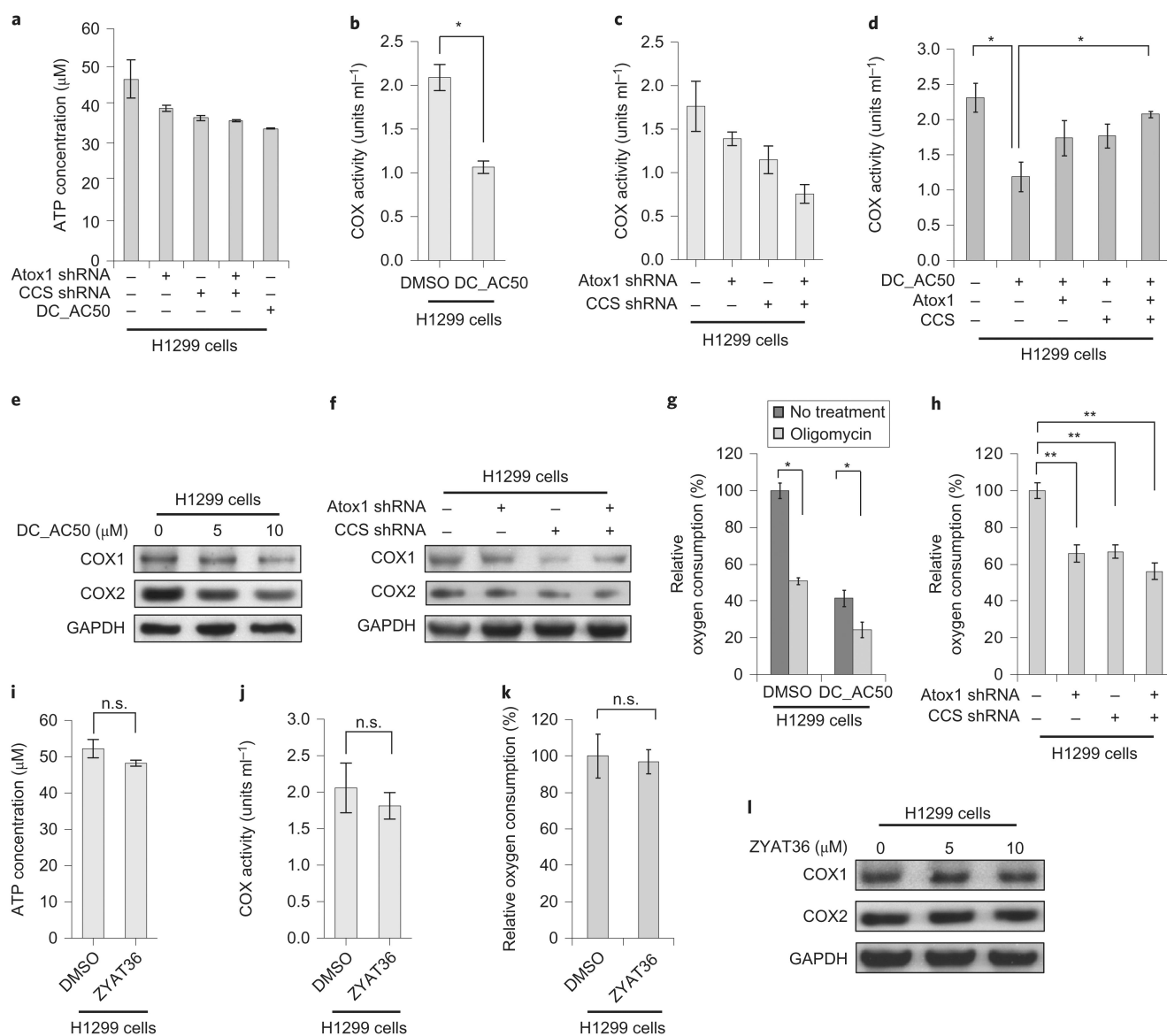
Figure 5. Treatment with DC_AC50 or Atox1/CCS knockdown decreases the cellular ATP level, COX activities and the rate of oxygen consumption in cancer cells

a, Atox1/CCS knockdown or **DC_AC50** (10 μM)-induced reduction of ATP levels in H1299 cells after 12 hours. **b,c**, **DC_AC50** (10 μM) or Atox1/CCS knockdown significantly lowers the COX activity in H1299 cells after 12 hours. **d**, The reduced COX activity by **DC_AC50** (10 μM) treatment could be rescued by Atox1/CCS overexpression. **e,f**, The expression levels of COX subunit 1 (COX1) and subunit 2 (COX2) decreased with different concentrations of **DC_AC50** (0-10 μM) or Atox1/CCS knockdown after 12 hours. **g,h**, Oxygen consumption decreased with **DC_AC50** (10 μM) or Atox1/CCS knockdown in H1299 cells after 12 hours. **i–l**, Treatment with the inactive control compound ZYAT36 (10 μM) did not affect the ATP level (**i**), COX activity (**j**), oxygen consumption (**k**) or the expression level of COX1,2 (**l**) in H1299 cells. Error bars, mean ± s.e.m., $n = 3$ biological replicates. $*P < 0.05$, $**P < 0.005$. GAPDH, glyceraldehyde-3-phosphate dehydrogenase.
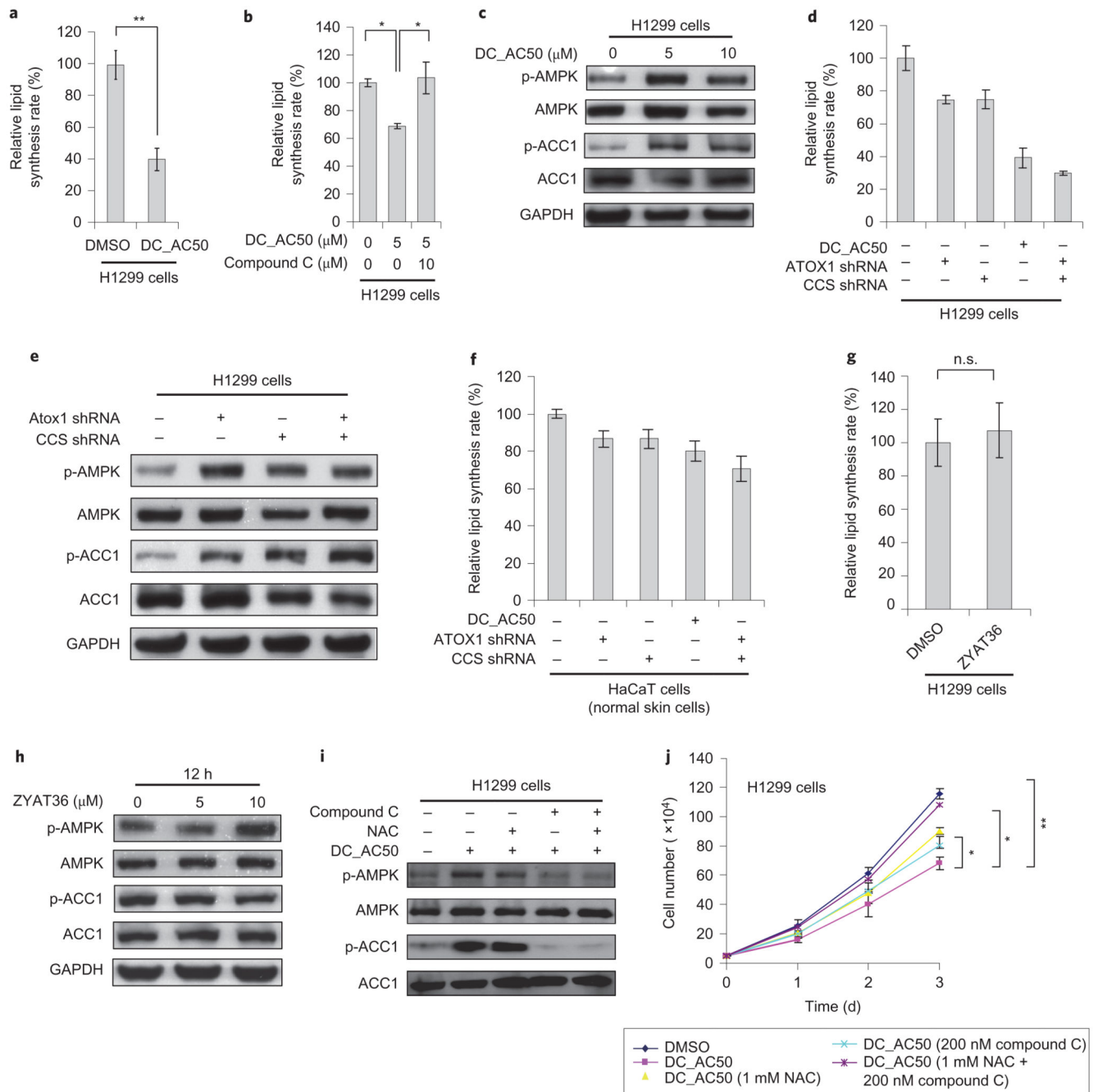
Figure 6. DC_AC50-induced mitochondria defects and decreased lipid biosynthesis through AMPK activation

a, Decreased lipid biosynthesis with **DC_AC50** (10 μM) treatment in H1299 cells. **b**, **DC_AC50**-induced lipid biosynthesis elevation can be rescued by 10 μM compound C (AMPK inhibitor). **c**, AMPK activation and ACC1 phosphorylation by a variety of **DC_AC50** (0–10 μM) treatments for 12 hours. **d,e**, Knockdown of Atox1 and CCS induced the reduction of lipid biosynthesis (**d**), AMPK activation and ACC1 phosphorylation (**e**) in H1299 cells after 12 hours. **f**, Knockdown of Atox1 and CCS in normal HaCaT cells did not

significantly reduce lipid biosynthesis after 12 hours. **g,h**, Treatment with the inactive control compound ZYAT36 (10 μM) did not induce a reduction of lipid biosynthesis (**g**), AMPK activation or ACC1 phosphorylation (**h**) in H1299 cells after 12 hours. **i**, AMPK activation and ACC1 phosphorylation by **DC_AC50** (10 μM) and rescue assays with compound C and NAC in H1299 cells after 12 hours. **j**, Cell-proliferation inhibition by **DC_AC50** (10 **μ**M) could be partially rescued by NAC or compound C. Treatment with both NAC and compound C almost completely rescued cell-proliferation inhibition by **DC_AC50** (10 μM) in H1299 cells. Error bars, mean ± s.e.m., $n = 3$ biological replicates. *$P < 0.05$, **$P < 0.005$.